Generalized theory of helicon waves. I. Normal modes

Francis F. Chen and Donald Arnush
Department of Electrical Engineering, University of California, Los Angeles, California 90095-1594

(Received 26 November 1996; accepted 6 May 1997)

The theory of helicon waves is extended to include finite electron mass. This introduces an additional branch to the dispersion relation that is essentially an electron cyclotron or Trivelpiece–Gould (TG) wave with a short radial wavelength. The effect of the TG wave is expected to be important only for low dc magnetic fields and long parallel wavelengths. The normal modes at low fields are mixtures of the TG wave and the usual helicon wave and depend on the nature of the boundaries. Computations show, however, that since the TG waves are damped near the surface of the plasma, the helicon wave at high fields is almost exactly the same as is found when the electron mass is neglected. © *1997 American Institute of Physics.* [S1070-664X(97)01309-8]

I. INTRODUCTION

Interest in plasma sources employing helicon wave excitation are of current interest because of their promise in providing the high density and uniformity needed for the fabrication of next-generation semiconductor circuits.[1,2] Analysis of recent experiments have depended on a simple treatment of helicon waves in which the electron mass m_e is taken to be zero,[3–7] so that $\delta \equiv \omega/\omega_c = 0$. At low magnetic fields, however, the electron cyclotron frequency ω_c can be the same order of magnitude as the wave frequency ω. For instance, for 27.12 MHz operation, $\delta \approx 0.25$ at $B_0 = 19$ G, a field low enough to permit economies in the design of plasma sources. Helicon theory with finite δ has been treated before by Klozenberg *et al.*[8] in their classic paper, by Bleven *et al.*,[9] and by Boswell.[10,11] Here we have assembled these various results and extended them in order achieve a single, coherent formulation of the theory, which can be readily used for comparison with ongoing experiments. In this paper (part I), complicating factors such as damping, antenna coupling, and density profiles have been neglected in order to bring out the physical ideas more clearly. The complete problem with extended computations are treated in a companion paper (part II). The analysis of part I is confined to the undamped, uniform-density case, and references to damping are made only to show the limitations of these idealized conditions. In part II, specific cases are computed to demonstrate the effects of plasma profiles, collisions, and antenna design.

II. GOVERNING EQUATIONS

In what follows, equilibrium quantities will be denoted by the subscript 0, while first-order perturbations (with no subscript) will be assumed to vary as $\exp i(m\theta + kz - \omega t)$. The z axis is aligned with the dc magnetic field: $\mathbf{B}_0 = B_0\hat{\mathbf{z}}$. Maxwell's equations are

$$\nabla \cdot \mathbf{B} = 0, \tag{1}$$

$$\nabla \times \mathbf{E} = i\omega \mathbf{B}, \tag{2}$$

$$\nabla \times \mathbf{B} = \mu_0(\mathbf{j} - i\omega\epsilon_0 \mathbf{E}) = -i\omega\epsilon_0\mu_0 \boldsymbol{\epsilon} \cdot \mathbf{E}. \tag{3}$$

The electron fluid equation of motion is

$$-i\omega m_e \mathbf{v} = -e(\mathbf{E} + \mathbf{v} \times \mathbf{B}_0) - m_e \nu \mathbf{v}, \tag{4}$$

where all dissipation mechanisms have been lumped into one phenomenological collision rate ν. We have omitted from Eq. (4) the magnetic viscosity term $n_0^{-1}\,\nabla \cdot \pi$ and the pressure term $n_0^{-1}\,\nabla p = n_0^{-1}\nabla[(n_0 + n)(KT_{e0} + KT_e)]$. The electron viscosity is important only when the electron Larmor radius is comparable to the radial wavelength of the waves, which is normally >1 cm for helicon waves; thus, for 3 eV electrons, $\nabla \cdot \pi$ can be neglected above ≈ 6 G. For TG (Trivelpiece–Gould) waves, however, wavelengths shorter than 1 mm are, in principle, possible. Such short-wavelength waves are not likely to exist in practice precisely because of finite-Larmor-radius (FLR) effects; the present theory is inadequate for these waves. Ionizing electrons of 15 eV energy have 1 cm Larmor radii below 13 G, and (FLR) effects are likely to be important for them at such low fields. Fortunately, their population should be so small that wave propagation, the subject of this paper, would not be affected. The zeroth-order pressure term $\nabla(n_0 KT_{e0})$ is important for discharge equilibrium,[4] but not for waves. The first-order part can be separated into four terms: ∇KT_e, $KT_e\,\nabla n_0/n_0$, $n\,\nabla KT_{e0}/n_0$, and $KT_{e0}\,\nabla n/n_0$. Since $\mathbf{E} \times \mathbf{B}$ motions are incompressible, n vanishes in a uniform plasma whenever FLR effects are negligible. The remaining term ∇KT_e can be neglected relative to the eE term, because fluctuations in KT_e are much less than $KT_e \approx 3$ eV, compared to wave electric potentials of >100 V, typically. In principle, the ∇p term can be included by using the warm-plasma theory of Allis, Buchsbaum, and Bers,[12] but the results are too cumbersome to be useful. Furthermore, finite T_e also engenders drift-wave effects in a nonuniform plasma, and treating these involves evaluating terms of comparable size in $v_0 \cdot \nabla v$ and $\nabla \cdot \pi$.[13] Fortunately, drift frequencies are well below helicon frequencies and should not be important in helicon wave propagation.

If we neglect ion motions, the plasma current is

$$\mathbf{j} = -en_0\mathbf{v}. \tag{5}$$

With the definitions

$$\omega_c = eB_0/m_e, \quad \delta_r = \omega/\omega_c, \quad \delta = (\omega + i\nu)/\omega_c, \tag{6}$$

Eq. (4) can be written as

$$\mathbf{E}=-\frac{B_0}{en_0}(i\delta\mathbf{j}+\hat{\mathbf{z}}\times\mathbf{j}). \tag{7}$$

The complex quantity δ can conveniently be replaced by its real part δ_r until the end, since Eq. (4) shows that ν appears only in combination with m_e; one only needs to replace m_e by $m_e(1+i\nu/\omega)$ in the final result.

At this point, we neglect the displacement current, so that Eq. (3) can be written as $\mathbf{j}=\mu_0\nabla\times\mathbf{B}$. Though displacement current can be included readily,[14] it is almost always negligible in experiment. Using Eqs. (3) and (7) to eliminate $\mathbf{j}$ and $\mathbf{E}$, we can write Eq. (2) as

$$i\omega\mathbf{B}=-\frac{B_0}{en_0\mu_0}\{i\delta\nabla\times\nabla\times\mathbf{B}+\nabla\times[\hat{\mathbf{z}}\times(\nabla\times\mathbf{B})]\}. \tag{8}$$

The last term reduces to $ik\nabla\times\mathbf{B}$. We now define

$$\omega_p^2\equiv ne^2/\epsilon_0 m_e, \quad k_s\equiv\omega_p/c \ \ (\text{``skin number''}),$$
$$\delta k_s^2=\omega n_0\mu_0 e/B_0\equiv k_w^2, \tag{9}$$

whereupon Eq. (8) becomes

$$\delta\nabla\times\nabla\times\mathbf{B}-k\nabla\times\mathbf{B}+k_w^2\mathbf{B}=0. \tag{10}$$

This is the equation we shall analyze. The quantity $k_w=k_s\sqrt{\delta}$ is simply the wave number of low-frequency whistler waves propagating along $\mathbf{B}$ in free space.

III. RELATION TO COLD-PLASMA THEORY

We have derived Eq. (10) in the most direct fashion, but as long as KT_e is neglected, it can also be derived from the standard theory of waves in a cold plasma. This formalism will permit an extension of the theory to include motions of an arbitrary number of species of ions, with displacement current also included. We follow the notation of Stix,[15] which is also adopted by Chen.[16] The total (plasma plus displacement) current in Eq. (3) is given in terms of the cold-plasma dielectric tensor by

$$\mathbf{J}=-i\omega\epsilon_0\begin{pmatrix} S & -iD & 0\\ iD & S & 0\\ 0 & 0 & P\end{pmatrix}\begin{pmatrix}E_x\\E_y\\E_z\end{pmatrix}. \tag{11}$$

This can be put in the form

$$\mathbf{J}=-i\omega\epsilon_0[P\mathbf{E}+iD\hat{\mathbf{z}}\times\mathbf{E}+(P-S)\hat{\mathbf{z}}\times\hat{\mathbf{z}}\times\mathbf{E}], \tag{12}$$

Eq. (12) is most easily inverted by writing out the components of $\mathbf{J}$ and solving directly for the components of $\mathbf{E}$. The result can be written in the form

$$-i\omega\epsilon_0\mathbf{E}=\alpha_c\mathbf{J}+i\alpha_h(\hat{\mathbf{z}}\times\mathbf{J})+\alpha_d[\hat{\mathbf{z}}\times(\hat{\mathbf{z}}\times\mathbf{J})], \tag{13}$$

where

$$\alpha_c=\frac{1}{P}, \quad \alpha_h=-\frac{D}{RL}, \quad \alpha_d=\frac{1}{P}-\frac{S}{RL}.$$

Here we have used $S^2-D^2\equiv RL$, arising from the definitions $S,D\equiv(R\pm L)/2$. In this form, it is clear that α_c represents the conduction or polarization current, $\alpha_{\rm H}$ the Hall current or $\mathbf{E}\times\mathbf{B}$ drift, and α_d the displacement current. The α_d term will be shown to vanish in the absence of j_d.

To reduce Eq. (13) to Eq. (7), we must evaluate the coefficients. For simplicity, we assume a single ion species, with characteristic frequencies Ω_p and Ω_c. The elements R, L are defined by

$$\frac{R}{L}=1-\frac{\omega_p^2/\omega^2}{1\mp\omega_c/\omega}-\frac{\Omega_p^2/\omega^2}{1\pm\Omega_c/\omega}, \tag{14}$$

where the first term is the contribution of the displacement current and cancels in the element D. In the limit $\Omega_c^2\ll\omega^2$ (with arbitrary $\omega_c^2/\omega^2>1$), the result is

$$D=-\frac{\omega_p^2\omega_c}{\omega^3}\frac{1}{1-\omega_c^2/\omega^2}. \tag{15}$$

Similarly, the ion term is found to be negligible in the evaluation of RL:

$$RL=1+\frac{\omega_p^2/\omega^2}{1-\omega_c^2/\omega^2}\left(\frac{\omega_p^2}{\omega^2}-2\right)\xrightarrow[j_d\to 0]{}\frac{\omega_p^4/\omega^4}{1-\omega_c^2/\omega^2}. \tag{16}$$

The terms ''1'' and ''2'' vanish when j_d is neglected. For $\Omega_c^2\ll\omega^2$, the element S becomes

$$S=1-\frac{\omega_p^2/\omega^2}{1-\omega_c^2/\omega^2}\left[1-\frac{\Omega_c}{\omega_c}\left(1-\frac{\omega_c^2}{\omega^2}\right)\right]$$
$$\approx 1-\frac{\omega_p^2/\omega^2}{1-\omega_c^2/\omega^2}\left(1+\frac{\omega_c\Omega_c}{\omega^2}\right)\to\frac{-\omega_p^2/\omega^2}{1-\omega_c^2/\omega^2}. \tag{17}$$

We see here that the frequency must be above the lower hybrid frequency in order for the ions to be neglected. In the limit $j_d\to 0$, Eqs. (16) and (17) give $S/RL=-\omega^2/\omega_p^2$, while

$$P\equiv 1-\omega_p^2/\omega^2\to-\omega_p^2/\omega^2. \tag{18}$$

Hence, the coefficient of the last term in Eq. (13) identically vanishes in the $j_d\to 0$ limit. Equations (15) and (16) give, in the $j_d\to 0$ limit,

$$\frac{D}{RL}=-\frac{\omega\omega_c}{\omega_p^2}. \tag{19}$$

With Eqs. (18) and (19), Eq. (13) becomes

$$\mathbf{E}=-\frac{\omega_c}{\epsilon_0\omega_p^2}(i\delta\mathbf{j}+\hat{\mathbf{z}}\times\mathbf{j}), \tag{20}$$

which is the same as Eq. (7).

IV. SEPARATION INTO HELICON AND CYCLOTRON WAVES

Equation (7) can be factored into[8]

$$(\beta_1-\nabla\times)(\beta_2-\nabla\times)\mathbf{B}=0, \tag{21}$$

where the separation constants β_1 and β_2 are the roots of

$$\delta\beta^2-k\beta+k_w^2=0. \tag{22}$$

Since k_w^2 is independent of mass, the only finite root β in the $m_e\to 0$ limit of this equation is

$$\beta=\frac{k_w^2}{k}=\frac{\omega}{k}\frac{\omega_p^2}{\omega_c c^2}=\frac{\omega}{k}\frac{n_0 e\mu_0}{B_0}\equiv\alpha, \tag{23}$$

the usual helicon dispersion relation.[3] For $\delta k_w^2 \ll k^2$, the two roots of Eq. (23) are well separated, with the approximate values

$$\beta_{1,2}=\frac{k}{2\delta}\left[1\mp\left(1-\frac{4\delta k_w^2}{k^2}\right)^{1/2}\right]$$
$$\approx\frac{k}{2\delta}\left[1\mp\left(1-\frac{2\delta k_w^2}{k^2}\right)\right]\approx\begin{cases}k_w^2/k\\ k/\delta\end{cases}. \tag{24}$$

Note that to this order the helicon wave is undamped, while the TG waves have all the damping. Previously reported damping rates were calculated[3,8] by perturbing this solution with the lowest-order finite-mass effects in the electrons' parallel motion.

The general solution of Eq. (21) is $\mathbf{B}=\mathbf{B}_1+\mathbf{B}_2$, where

$$\nabla\times\mathbf{B}_1=\beta_1\mathbf{B}_1, \quad \nabla\times\mathbf{B}_2=\beta_2\mathbf{B}_2. \tag{25}$$

Taking the curl of these equations and using Eq. (1), we obtain a vector Helmholtz equation for each:

$$\nabla^2\mathbf{B}_1+\beta_1^2\mathbf{B}_1=0, \quad \nabla^2\mathbf{B}_2+\beta_2^2\mathbf{B}_2=0. \tag{26}$$

From these wave equations, we see that the β's are effectively total wave numbers. The root β_1 corresponds to the usual helicon wave of Eq. (23), which we shall call the H wave. From Eq. (24), we see that the new root β_2 gives a wave with the approximate dispersion relation

$$\beta=k_\parallel\omega_c/\omega=\beta\cos\theta\,\omega_c/\omega, \tag{27}$$

where θ is the angle of propagation relative to $\mathbf{B}_0$. This wave, with frequency $\omega=\omega_c\cos\theta$, is evidently an electron cyclotron wave, first treated with cylindrical boundaries by Trivelpiece and Gould;[17] we shall call this the TG wave. The remainder of this paper concerns the coupling of these two waves; and for simplicity, the damping will be neglected, so that $\delta=\delta_r$.

The relation of Eq. (22) between k and β can also be written as

$$k=\frac{\delta}{\beta}(\beta^2+k_s^2). \tag{28}$$

The solution of the wave equations (26) in cylindrical geometry can be expressed[3] in terms of Bessel functions $J_n(\mathrm{Tr})$, where the transverse wave number T is defined by

$$T_j^2=\beta_j^2-k^2, \quad j=1,2. \tag{29}$$

Differentiation of Eq. (28) yields a minimum value of k given by

$$k_{\min}=2\,\delta k_s. \tag{30}$$

If T is real, there is also a maximum value of k occurring when $T=0$, $k=\beta$:

$$k_{\max}=\left(\frac{\delta}{1-\delta}\right)^{1/2}k_s. \tag{31}$$

These two limits are equal when $\delta=\omega/\omega_c=\frac{1}{2}$. At magnetic fields so low that $\delta>\frac{1}{2}$, only one propagating wave can exist; the helicon branch disappears. An example of a k-β diagram is shown in Fig. 1. Similar diagrams showing the minimum in k were first shown by Boswell.[10,11] For each k, the value of β to the left of the minimum is β_1 (H wave), and the value to the right is β_2 the (TG wave). Note that for the H wave the lowest radial mode (smallest β) corresponds to the shortest parallel wavelength (largest k), while the opposite is true for the TG wave. For B_0 less than 19 G, only the TG wave can propagate at 27 MHz.

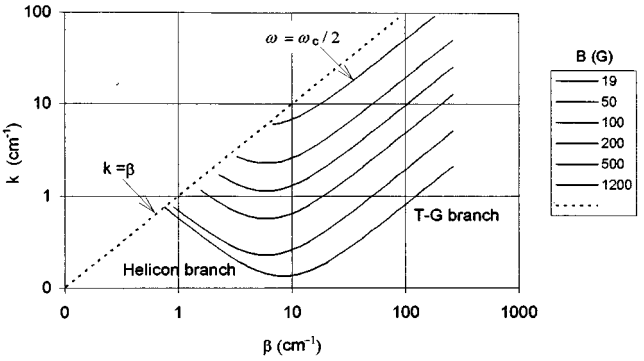

FIG. 1. The k-β curves for $n_0=2\times10^{13}$ cm^{-3} and various values of the magnetic field, listed in the legend in the same order as they appear. Unless otherwise specified, computations are for 27.12 Mhz, a 2.5 cm tube radius, and the $m=+1$ azimuthal mode.

V. CONDUCTING BOUNDARY

This boundary condition is rather unrealistic, since in actual experiments a quartz or glass tube is used so as not to shield out the antenna fields, and in any case the region of high density does not extend all the way to the wall. The reason for treating this case is to make contact with early theories of helicon waves.[3] The solution of Eq. (26) that is finite on the axis for either wave in a uniform plasma filling a conducting cylinder of radius a has been given previously,[3,8]

$$B_{rj}=A_j[(\beta_j+k)J_{m-1}(T_jr)+(\beta_j-k)J_{m+1}(T_jr)], \tag{32}$$

$$B_{\theta j}=iA_j[(\beta_j+k)J_{m-1}(T_jr)-(\beta_j-k)J_{m+1}(T_jr)], \tag{33}$$

$$B_{zj}=-2iA_jT_jJ_m(T_jr), \quad j=1,2, \tag{34}$$

where T_j is given by Eq. (29), and m is the azimuthal mode number. From Eqs. (25) and (3) with the displacement current neglected, we see that $\mathbf{j}$ is parallel to $\mathbf{B}$:

$$\mathbf{j}_j=(\beta_j/\mu_0)\mathbf{B}_j. \tag{35}$$

Equation (20) then gives

$$E_{zj}=-\frac{i\omega m_e}{n_0e^2}j_{zj}=-\frac{i\omega m_e}{n_0e^2}\frac{\beta_j}{\mu_0}B_{zj}. \tag{36}$$

The other components of $\mathbf{E}$ can be found from Eq. (2):

$$E_r=\frac{\omega}{k}B_\theta-\frac{i}{k}E_z', \quad E_\theta=\frac{m}{kr}E_z-\frac{\omega}{k}B_r. \tag{37}$$

In the zero-mass limit, E_z vanishes identically for the H wave (the only one in that case), and only one other boundary condition needs to be satisfied; namely, $E_\theta=0$ at $r=a$. From Eq. (37), this means that $B_r=0$. For an insulating boundary, the boundary condition would be $j_r=0$, which, by

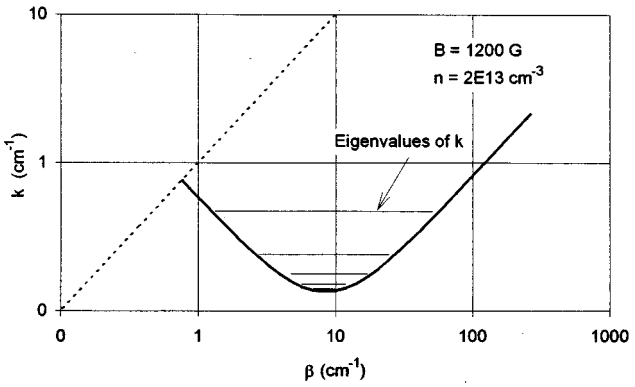

FIG. 2. An example of quantized k values when the plasma is confined by conducting walls.

Eq. (35), also means that $B_r=0$. Thus, in this particularly simple case of $m_e=0$, there is only one universal boundary condition, which applies to either type of boundary:

$$B_{r1}=A_1[(\beta_1+k)J_{m-1}(T_1a)+(\beta_1-k)J_{m+1}(T_1a)]=0. \tag{38}$$

This is the condition used by all previous authors, and we shall refer to it as the *single-BC*, or *1-BC*, case.

When m_e cannot be neglected, E_z exists by virtue of electron inertia, even in the collisionless case. Equation (36) then requires that $\beta_j B_{zj}$ vanish at the boundary, or, from Eq. (34), that $\beta_j J_m(T_j a)=0$. Clearly, this condition is not consistent with Eq. (38), so that a pure H or TG wave cannot satisfy both boundary conditions by itself. Since we started with a second-order vector equation in Eq. (10), both waves must exist, coupled at the boundary, in order that their amplitude ratio can supply the required degree of freedom. (In the inhomogeneous case treated in part II, this coupling or mode conversion occurs everywhere where there is a density gradient.) Setting $j_{z1}+j_{z2}=0$, we obtain from Eqs. (36) and (34) the required amplitude ratio,

$$\frac{A_2}{A_1}=-\frac{\beta_1 T_1 J_m(T_1a)}{\beta_2 T_2 J_m(T_2a)}. \tag{39}$$

With $E_z=0$, Eq. (37) then requires B_r to vanish to satisfy $E_\theta=0$. Setting $B_{1r}+B_{2r}=0$, we obtain from Eq. (32) the amplitude ratio

$$\frac{A_2}{A_1}=-\frac{[(\beta_1+k)J_{m-1}(T_1a)+(\beta_1-k)J_{m+1}(T_1a)]}{[(\beta_2+k)J_{m-1}(T_2a)+(\beta_2-k)J_{m+1}(T_2a)]}, \tag{40}$$

where $\beta_j(k)$ is given by Eq. (24) and $T_j[k,\beta(k)]$ by Eq. (29). For given plasma parameters n_0 and B_0, Eqs. (39) and (40) can be satisfied simultaneously only for certain values of k. The possible values of k are now quantized, as is shown by the example of Fig. 2. The complete boundary condition is

$$\begin{aligned}&[(\beta_1+k)J_{m-1}(T_1a)+(\beta_1-k)J_{m+1}(T_1a)]\\&\quad=[(\beta_2+k)J_{m-1}(T_2a)+(\beta_2-k)\\&\qquad\times J_{m+1}(T_2a)]\,\frac{\beta_1 T_1 J_m(T_1a)}{\beta_2 T_2 J_m(T_2a)},\end{aligned} \tag{41}$$

where the right-hand side (rhs) vanishes in the 1-BC case. For values of k near $k_{\max}$, $\beta_1 T_1$ is much smaller than $\beta_2 T_2$, and the rhs is so small that the dispersion relation for the helicon branch is insignificantly affected by the inclusion of finite m_e and, hence, of finite E_z. An example of this is shown in Fig. 5 below. In Eq. (36), note that E_{z2}/B_{z2} is proportional to β_2, which is much larger than β_1 when B_0 is large. This shows that the Trivelpiece–Gould mode is electrostatic in character, as is well known. It is at low magnetic fields, when β_2 and β_1 are comparable, that the electromagnetic part of the TG wave cannot be neglected.

In Fig. 2 the highest eigenvalue of k corresponds to the lowest radial helicon mode and the highest radial TG mode. In this case there are six radial modes, $n=1-6$, though the $n=5$ and 6 modes at the bottom of the parabola cannot be seen on this scale. Because of damping, only the $n=1$ mode is normally observed in the experiment,[18] though a small amplitude of the $n=2$ mode has been invoked to explain spatial beats in the wave pattern.[19] For low values of B_0, the effective potential well is shallow, and only one or two radial modes can be found. Though the number of eigenvalues k and their magnitudes are mathematically determinate, the closely spaced eigenvalues for the high radial modes have little physical significance. To show this, we have plotted in Fig. 3 the two sides of Eq. (41) for a large-B_0 case. It is seen in Fig. 3(a) that the lowest radial modes of the helicon wave at large k are unaffected by the rhs of Eq. (41), representing the finite-m_e correction to the boundary conditions. In Figs. 3(b) and 3(c), however, it is clear that, for the high radial modes at small k, the lhs=0 and lhs=rhs conditions are greatly affected by a small change in n_0. These roots of Eq. (41) are so sensitive to k that they could not be found with prepackaged root-finding routines such as in Microsoft Excel and had to be computed by hand. The reason for this unphysical result is that we have neglected all damping, so that the TG wave extends all the way to the axis, where its phase is determined. As k is varied, the values of β_1 and β_2, and hence of T_1 and T_2, change in opposite directions; and only when the values of B_r and j_z for the two waves cancel at $r=a$ is there a solution. In practice, at high densities, the TG mode is damped well before it reaches the axis, so that its phase at $r=0$ is arbitrary; then one would expect that any value of k can satisfy the boundary condition. In this sense, the conducting boundary condition gives misleading results; the insulating boundary conduction gives a continuous k spectrum in the undamped limit, more closely resembling the full solution that includes damping and density falloff at the edge.

In Fig. 2 it is clear that the TG wave has very short radial wavelength when it is coupled to the lowest radial mode of the helicon wave. In that case, the TG wave can be expected to be damped within a millimeter or two of the surface and to affect only the energy deposition, but not the measured wave

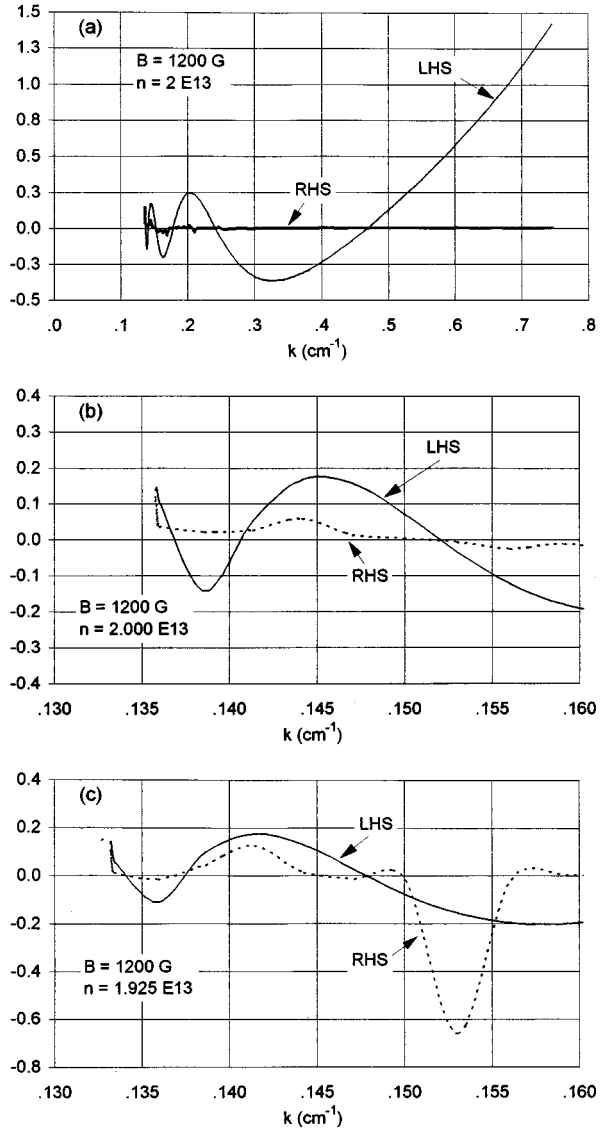

FIG. 3. An example of the determination of the eigenvalues of k for conducting boundaries. In (a), the right- and left-hand sides of Eq. (41) are plotted between $k_{\min}$ and $k_{\max}$, showing that the zero crossings of the lhs are not greatly affected by the rhs for the short-axial-wavelength modes (the lowest helicon radial modes). In (b), the abscissa has been expanded to show the high radial modes. The sensitivity of the rhs to a small change in density is shown in (c).

profiles in the interior. This is shown in Fig. 4(a), where it is seen that the simple $m_e=0$ theory used previously correctly predicts the behavior of the H wave if the TG component is neglected. On the other hand, for high radial modes near the bottom of the parabola of Fig. 2, the H and TG waves have comparable radial wavelengths, and the TG component cannot easily be dismissed. Figure 4(b) shows that previous theory closely approximates the H component but that the TG component is dominant in this case. Furthermore, as shown in Fig. 4(b) neglecting the $E_z=0$ boundary condition would affect the calculated wave profiles for these high radial modes, if they are at all observable.

Though both the H and TG waves are needed in a mathematical sense to satisfy the boundary conditions on B_r and E_z, the latter condition is not a stringent one. Figure 5 shows

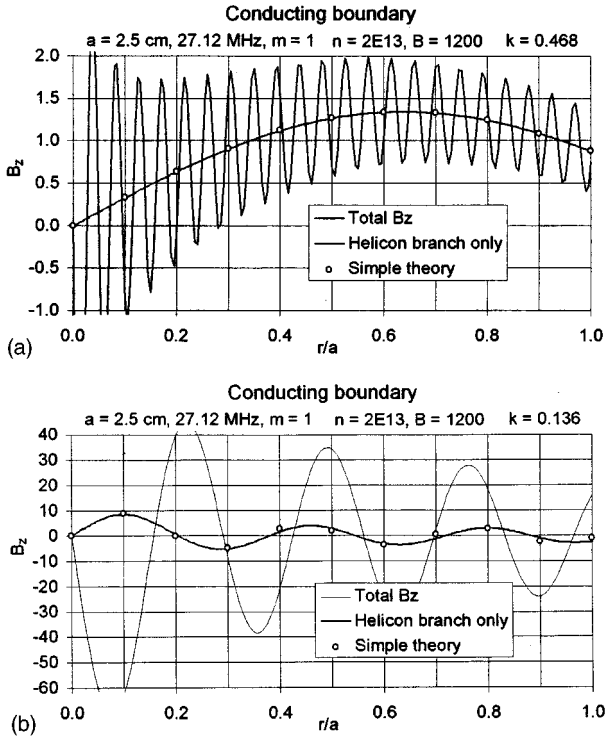

FIG. 4. The radial profile of B_z for a high-field case for (a) the lowest and (b) the highest ($n=6$) radial H mode. The heavy line is for the H wave alone, without the TG component, and the points are calculated from simple $m_c=0$ theory.

the effect of neglecting the right-hand side of Eq. (41), thus effectively ignoring the boundary condition on E_z. It is seen that the shape of each wave individually is not sensitive to the E_z boundary condition, though the ratio of amplitudes is.

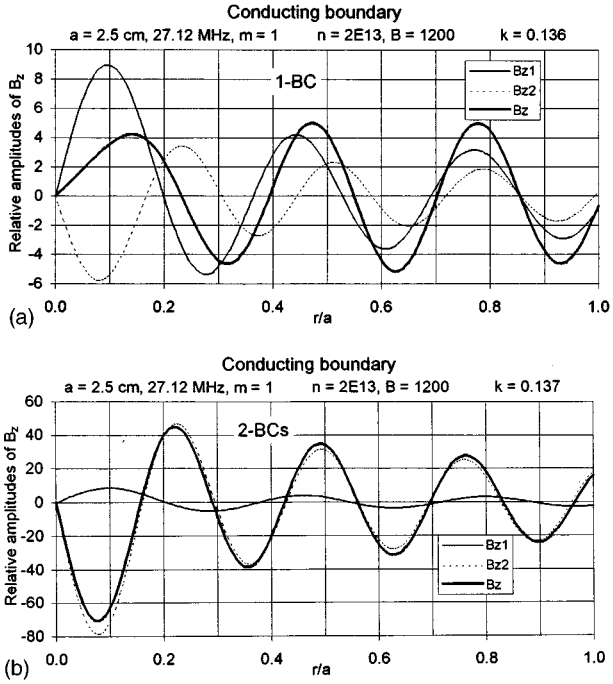

FIG. 5. The radial profile of B_z for a high-field case when the $E_z=0$ boundary condition is (a) neglected and (b) included. The total B_z is shown, together with the H (B_{z1}) and TG (B_{z2}) contributions.

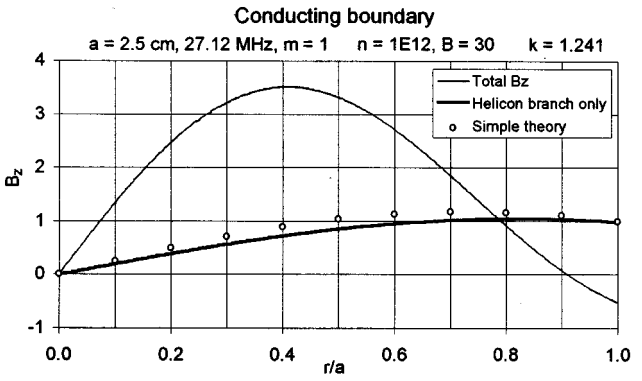

FIG. 6. The radial profile of B_z for a low-field case ($\omega/\omega_c=0.32$) when only one radial mode is possible. The heavy line is for the H wave alone, without the TG component, and the points are calculated from simple $m_c=0$ theory.

In this sense, the dispersion relation is factorable, and the H and TG waves are approximately uncoupled, a conclusion reached earlier by Shamrai and Taranov[20] for conducting boundaries. On the other hand, at low magnetic fields such that only one eigenvalue of k is possible, with $\beta_1\approx\beta_2$, one would expect the H and TG waves to be strongly coupled. That case is explored in detail in part II. An example is shown in Fig. 6, where the coupled waves have a different profile than either wave alone, though simple theory correctly predicts the behavior of the H component.

Note that the relative amplitudes of the H and TG waves, as they would be measured with probes, do not convey the importance of the TG wave to maintaining the discharge. The absorption of rf energy depends on $\mathbf{j}\cdot\mathbf{E}$, and from Eqs. (35)–(37) we see that this quantity contains a factor of β or β^2. Because of its larger value of β, the TG wave can have a large role in heating, even if its amplitude is relatively small.

VI. INSULATING BOUNDARY

We consider here an infinitely long, uniform plasma column confined by an insulating tube of inner radius a. For simplicity, the dielectric constant of the insulator is taken to be unity; the small phase shift introduced by a real glass or quartz tube does not affect our results. Surrounding the tube at some radius b is a conducting cylinder, where E_θ and E_z must vanish. The waves in the vacuum region are highly evanescent, since the k of the helicon waves is larger than $k_0\equiv\omega/c$ by typically two orders of magnitude. Therefore, the waves in the plasma are insensitive to b as long as $d=b-a$ is larger than some fraction of the plasma radius. We can therefore take $b\to\infty$. This approximation will be removed in part II.

For the vacuum region (subscript 3), setting $\mathbf{j}=0$ in Eq. (3) changes Eq. (26) to

$$\nabla^2\mathbf{B}_3+k_0^2\mathbf{B}_3=0, \tag{42}$$

and Eq. (29) to

$$T^2=k_0^2-k^2\equiv-T_3^2\approx-k^2. \tag{43}$$

Since $k^2\gg k_0^2$, T^2 is negative in the exterior region. The change in sign causes the Bessel functions to have imaginary arguments. Rejecting the solution that diverges as $r\to\infty$, we find that the functions $J_n(\mathrm{Tr})$ in Eqs. (32)–(34) are replaced by $K_n(T_3r)$, where T_3 is positive. The normal component B_r is continuous at $r=a$. The tangential components B_θ and B_z must also be continuous, since a real plasma cannot carry an infinitesimally thin surface current. Continuity of the tangential components of $\mathbf{E}$ require that E_z be continuous; E_θ is then automatically continuous from Eq. (2). No condition is imposed on E_r or B_z' since a surface charge can, in general, exist. The matching of the interior and exterior solutions is most easily done with the circularly polarized components B^R and B^L, where

$$\sqrt{2}B^R=B_r-iB_\theta,\quad \sqrt{2}B^L=B_r+iB_\theta. \tag{44}$$

The interior solution of Eqs. (32)–(34) can be written as

$$B_j^R=\sqrt{2}(\beta+k)A_jJ_{m-1}(T_jr), \tag{45}$$

$$B_j^L=\sqrt{2}(\beta-k)A_jJ_{m+1}(T_jr), \tag{46}$$

$$B_{jz}=-2iT_jA_jJ_m(T_jr). \tag{47}$$

The exterior solution is

$$B_3^R=\sqrt{2}C_1K_{m-1}(T_3r), \tag{48}$$

$$B_3^L=\sqrt{2}C_2K_{m+1}(T_3r), \tag{49}$$

$$B_{3z}=-i(T_3/k)(C_1+C_2)K_m(T_3r), \tag{50}$$

where $T_3^2=k^2-k_0^2$. The coefficients of the B_z components were found from Eq. (1). We now normalize to the amplitude of the H wave, setting $A_1=1$. Matching the inside and outside components of $\mathbf{B}$ at $r=a$ gives the amplitudes A_2, C_1, and C_2 relative to A_1. The result is

$$C_1=f_1+f_2A_2,\quad C_2=g_1+g_2A_2, \tag{51}$$

$$A_2=-(f_1+g_1-h_1)/(f_2+g_2-h_2), \tag{52}$$

$$\begin{Bmatrix} f_j \\ g_j \end{Bmatrix}=(\beta_j\pm k)\,\frac{J_{m\mp1}(T_ja)}{K_{m\mp1}(T_3a)},\quad h_j=\frac{2k}{T_3}\left(T_j\,\frac{J_m(T_ja)}{K_m(T_3a)}\right). \tag{53}$$

For any given value of k, Eq. (52) gives the ratio of amplitudes of the TG and H waves in the plasma, and Eq. (51) gives the amplitude and phase of the wave outside.

We now apply the condition on E_z. From Eqs. (20), (35), and (47), we find that E_z in the interior region (with displacement neglected) can be written as

$$E_z^{\mathrm{in}}=-\frac{2c^2}{\omega}\,\frac{k_0^2}{k_s^2}\,[A_1\beta_1T_1J_m(T_1r)+A_2\beta_2T_2J_m(T_2r)]. \tag{54}$$

In the exterior region, since there is no conduction current, E_z exists by virtue of the displacement current only. From Eqs. (3), (48), and (49), we find

$$E_z^{\mathrm{out}}=\frac{c^2}{\omega}\,T_3(C_1-C_2)K_m(T_3r). \tag{55}$$

Comparing this to E_z^{in}, we see that the small factor k_0^2/k_s^2 makes C_1-C_2 essentially zero, meaning that the displace-

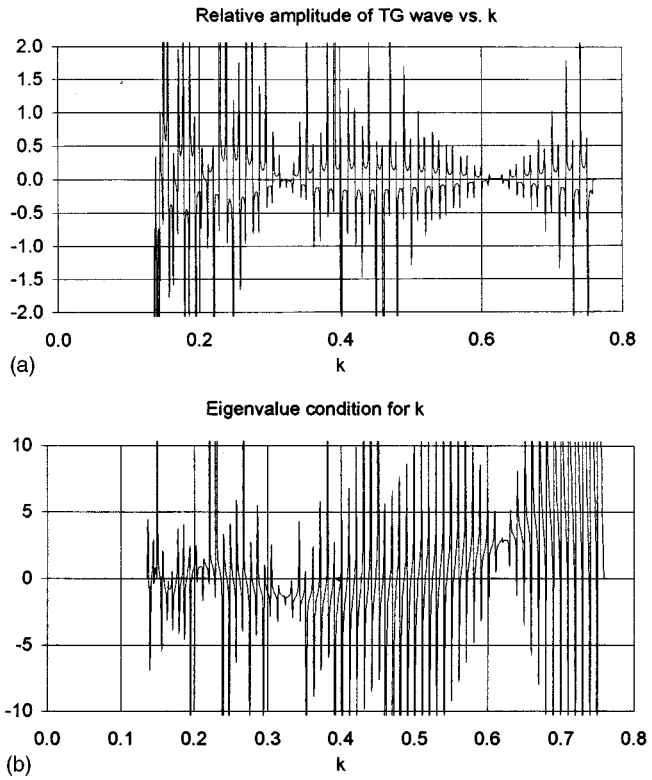

FIG. 7. For an insulating boundary, (a) the relative amplitude A_2/A_1 of the TG and H waves versus k, and (b) the condition determining the eigenvalues of k, which occur at each zero crossing.

ment current is negligible, even in the exterior region. Solving for C_1-C_2 from continuity of E_z at $r=a$ and making use of Eq. (53), we find

$$C_1-C_2=-\frac{k_0^2}{kk_s^2}\,(\beta_1 h_1+A_2\beta_2 h_2), \tag{56}$$

where A_1 has been normalized to unity. Equation (51) requires, however, that

$$C_1-C_2=f_1-g_1+A_2(f_2-g_2). \tag{57}$$

These conditions are not compatible with each other except for certain values of k. From Eqs. (52), (56), and (57), the eigenvalue equation for k can be written as

$$-A_2=\frac{f_1+g_1-h_1}{f_2+g_2-h_2}=\frac{f_1-g_1+\lambda\beta_1 h_1}{f_2-g_2+\lambda\beta_2 h_2}, \tag{58}$$

where $\lambda\equiv k_0^2/kk_s^2$. For large B_0, one sees from Fig. 1 that the lowest radial modes of the helicon wave are coupled to TG modes of large β. In that case, the argument T_2a of the Bessel functions in f_2, g_2, and h_2 is very large, and these functions oscillate rapidly with k. The first equality in Eq. (58) then shows wild fluctuations of $A_2(k)$, as shown in Fig. 7(a). When $A_2=0$, the H wave exists alone; and when $A_2\to\infty$, the TG wave exists alone. Shamrai and Taranov[21] has called these points *antiresonances*. However, the allowed values of k must also satisfy the second equality in Eq. (58). This condition is shown in Fig. 7(b), which also fluctuates rapidly with k. However, both numerators of the two fractions in Eq. (58) cannot vanish simultaneously, nor can both denominators; hence, antiresonances cannot occur in the absence of damping. The general formulation in part II will make this point self-evident.

Thus, for large B_0, an almost continuous spectrum of k's between $k_{\min}$ and $k_{\max}$ is possible in the case of an insulating boundary. As explained earlier, the discreteness of the spectrum is caused by the theoretical behavior of the TG wave at $r=0$. Since in practice TG waves of short radial wavelength are rapidly damped, the spectrum of H waves in the interior will be essentially continuous between $k_{\min}$ and $k_{\max}$. This point can be shown rigorously by replacing the Bessel functions of argument T_2a in Eq. (58) with their asymptotic expansions and giving T_2 a small imaginary part; we omit the details here. If we ignore the TG component, we shall see that the H component itself is well behaved at high fields, and its radial profile is insensitive to the nature of the boundary. This situation is changed if B_0 is low that β_1 and β_2 are of comparable magnitude. Then the H and TG waves are strongly coupled at all radii, and there will be only one or two discrete values of k.

Figure 8 shows an example of the wave fields, for a high radial mode at large B_0, in which both the H and TG waves are important. Figure 8(a) shows the total B_z field, and Figs. 8(b)–8(d) give the components of **B** for each wave separately. The external field happens to be small in this case, but it is not always so.

Figures 9 and 10 compare the wave fields for conducting and insulating boundary conditions for nearly equal values of k, values that are eigenvalues in each case. Figure 9(a) shows the B_z field for an intermediate value of k. The TG wave is dominant here because of the large factor T_2 in Eq. (47). The boundary condition affects the relative magnitudes of the H and TG waves but not their radial profiles, since that is determined by the value of k. This is demonstrated in Fig. 9(b), which shows the profile of the H branch alone. Figure 10 shows an example for a magnetic field so low that only one value of k is allowed under either boundary condition, and the H and TG branches contribute comparably to the total field. Since the eigenvalues of k in the two cases are not the same, a slight difference can be seen in the profiles of both the total B_z and that of the H branch alone.

VII. THE k-ω AND n-B DIAGRAMS

Up to now we have considered the possible values of k for given plasma parameters n_0 and B_0 and given frequency ω. If ω is varied for a given plasma, k can be found by solving Eq. (41) for a conducting boundary to obtain the usual form of a dispersion relation: $\omega(k)$ or $k(\omega)$. For an insulating boundary, the entire range of k between $k_{\min}$ and $k_{\max}$, Eqs. (30) and (31), is densely sampled if B_0 is large. Plots of the range of k versus frequency f and the eigenvalues of k for the first two radial modes in the conducting-boundary case are shown in Fig. 11(a) for a high magnetic field. The sensitivity to density is illustrated by comparing Figs. 11(a) and 11(b). Figure 11(c) shows a low-field case in which there is only one radial mode with either boundary

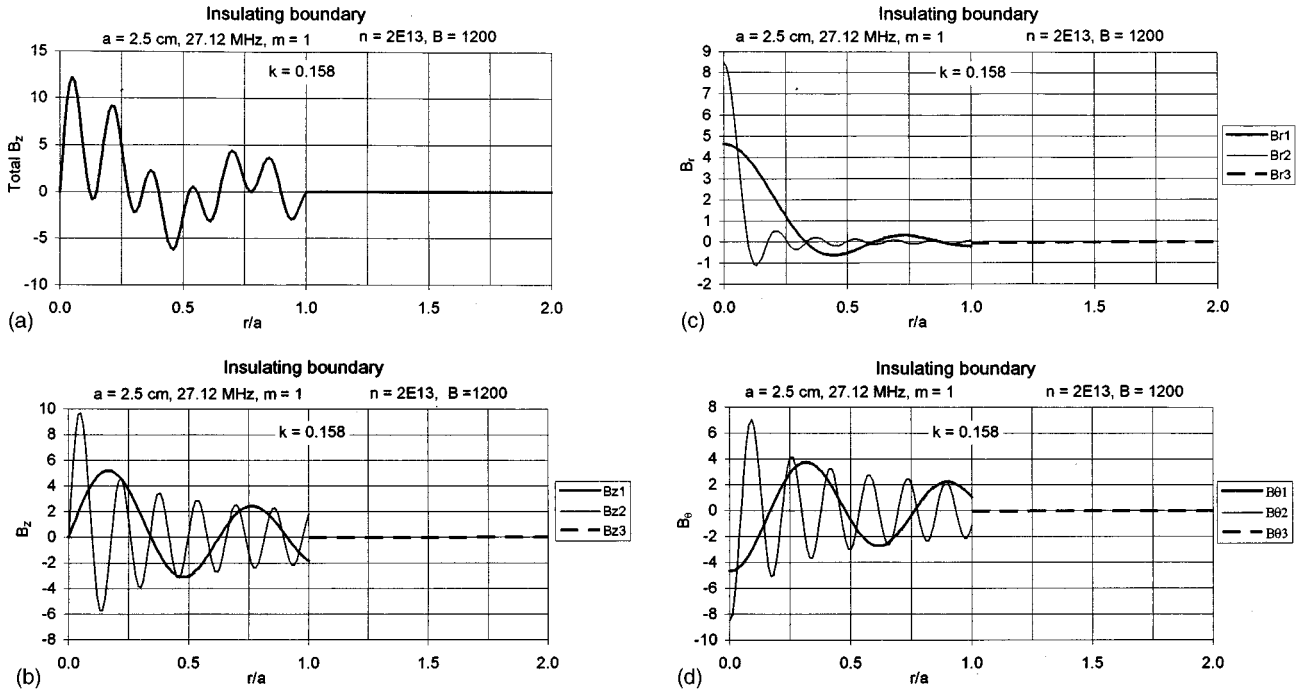

FIG. 8. The components of the wave field inside and outside a plasma confined by an insulating boundary for a typical case: (a) the total B_z field; (b)–(d) the B_z, B_r, and B_θ fields of the H (heavy line) and TG (light line) contributions shown separately.

condition. The k values are very similar. Note that, with an assumed tube radius of 2.5 cm, operation at 27.12 MHz is more likely to be in the linear region of the k-ω diagram than operation at 13.56 MHz.

Experimentally, for fixed ω and B_0, a preferred range of k may be determined by the excitation mechanism, such as the length of the antenna or a phase velocity resonance. In that case, the plasma density will adjust itself to a value that fits the dispersion relation. For a conducting boundary, Eq.

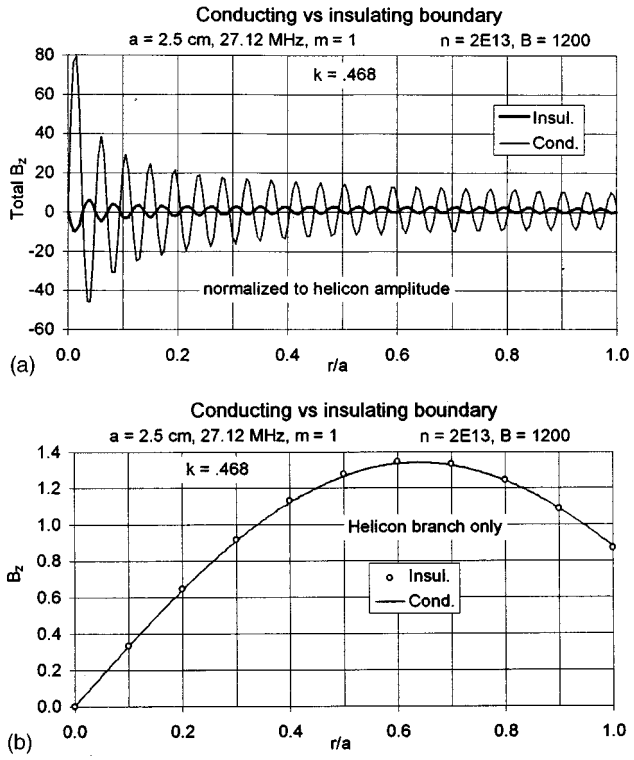

FIG. 9. A comparison of the B_z profiles computed for conducting and insulating boundary conditions. In (a) the coupled waves are shown, the vertical scale indicating the amplitude of the total field relative to the helicon branch. In (b) the H component alone is shown.

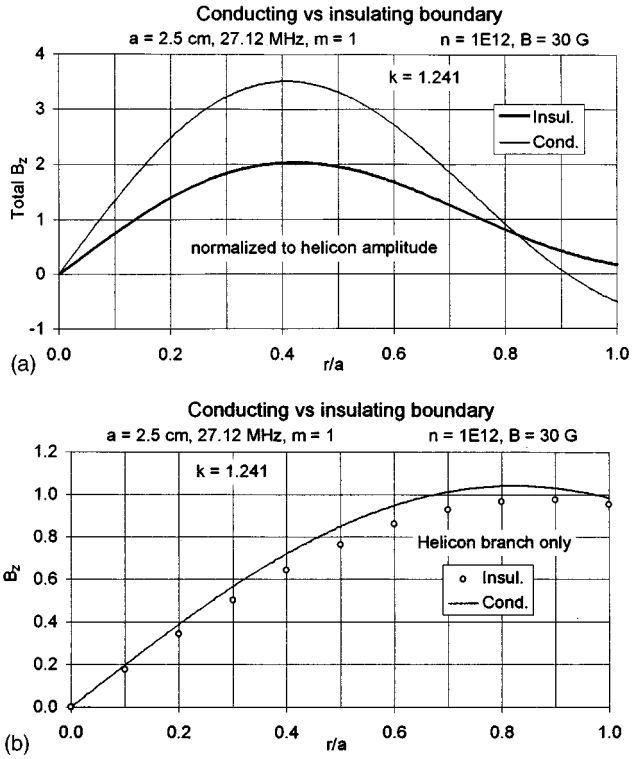

FIG. 10. The same as Fig. 9 for a case of a low magnetic field.

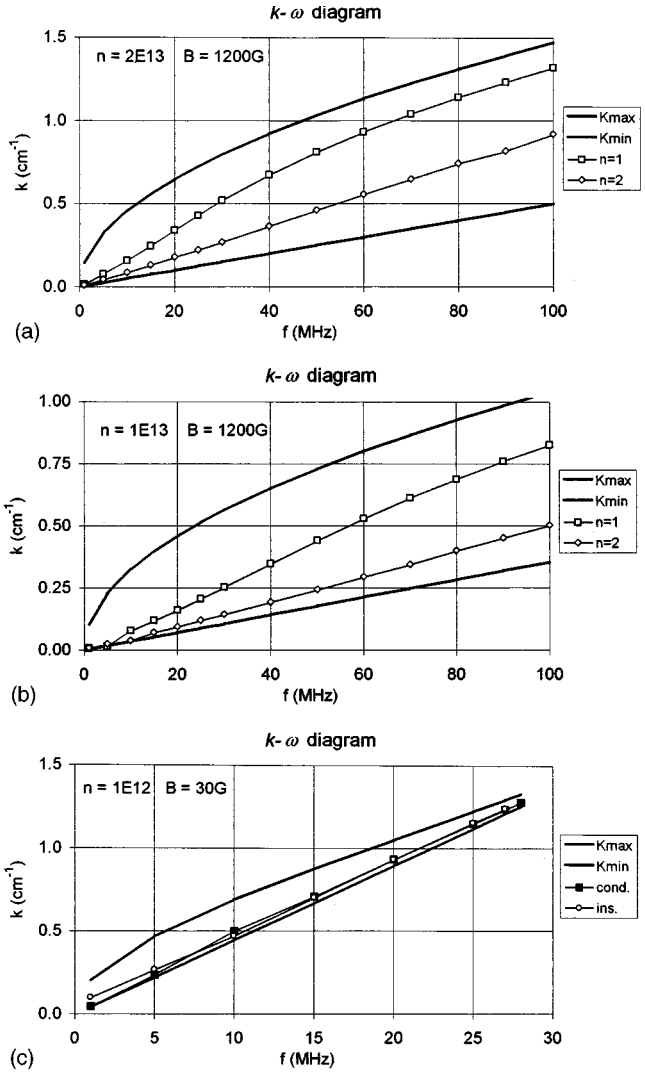

FIG. 11. Examples of k-ω diagrams. The lines with points show the two highest eigenvalues of k in a 2.5 cm conducting tube; the heavy lines show the range of k that is possible in an insulating tube. (a) and (b) A high-field case for two different densities. (c) A low-field case with $\omega/\omega_c = 0.32$, in which k is quantized even for an insulating boundary.

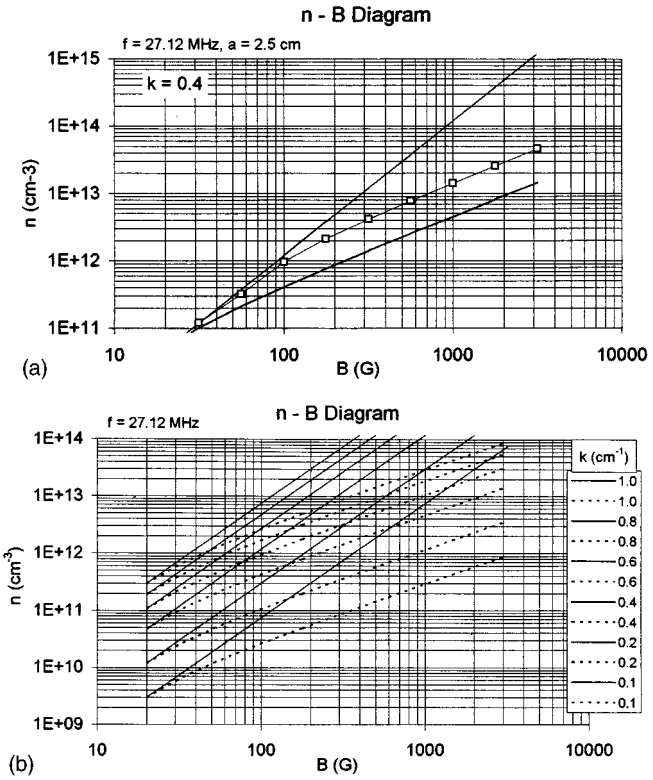

FIG. 12. Examples of n-B diagrams. (a) The line with points shows eigenvalues of n for the lowest radial mode in a 2.5 cm conducting tube; the heavy lines show the range of n that is possible in an insulating tube. (b) The k variation of the maximum (solid) and minimum (dashed) values of n_0 in an insulating tube.

(41) gives the eigenvalue of n_0, while, for an insulating boundary, Eqs. (30) and (31) give the possible range of n_0. This is best obtained by fixing n_0 (or k_s) and solving for the range of B_0 (or δ) from $k_{\min} = 2\delta k_s < k < k_s[\delta(1-\delta)]^{1/2} = k_{\max}$. An example is shown in Fig. 12(a) for an intermediate value of k. We see that $n_{\max}$ varies as B_0^2, as predicted by Eq. (30), while $n_{\min}$ varies as B_0, as predicted by Eq. (31). The conducting boundary solution shows that n_0/B_0 is constant, as given by $m_e = 0$ theory,[3] but only for fields exceeding 100 G. Figure 13(b) shows $n_{\max}$ and $n_{\min}$ vs B_0 for various values of k.

VIII. TRANSITION TO ZERO-FIELD DISCHARGES

In semiconductor processing, Inductively Coupled Plasma discharges (ICPs) without a dc magnetic field are commonly used. These include plasma sources with helical antennas, surrounding a cylindrical tube, usually with a Faraday shield, and Transformer Coupled Plasmas (TCPs), which employ a spiral coil separated from the plasma by a flat quartz plate. If the dc magnetic field of a high-field helicon discharge is reduced to zero, the transition to an ICP occurs in a complicated way. As we have seen, if B_0 is reduced so that $\delta = \omega/\omega_c$ increases from a small value to the order of but still less than $\frac{1}{2}$, a strongly coupled H–TG mode can propagate in the plasma at a discrete value of k. As δ is increased beyond $\frac{1}{2}$, an intermediate situation occurs, where, for $k < k_s$, a propagating TG wave is coupled to an evanes-

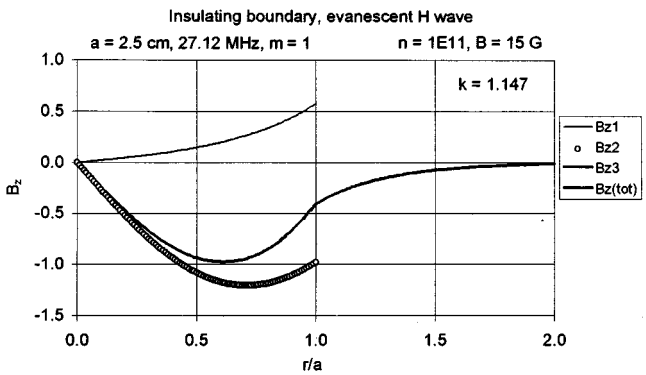

FIG. 13. Example of a TG wave (B_{z2}) coupled to an evanescent H wave (B_{z1}) at low fields such that $\omega/\omega_c > \frac{1}{2}$. There was only one eigenvalue of k in this case, and the ratio k/k_s was 1.93.

cent H wave. For very large δ, both waves are evanescent with a skin depth $1/k_s$, as in the ICP and TCP.

To explore the intermediate regime, we first square Eq. (24) for the collisionless case and insert into Eq. (29) to obtain

$$T^2 = -k_s^2 - k^2\left(1 - \frac{1}{2\delta^2}\right) \mp \frac{2kk_s}{\delta}\left(\frac{k^2}{4\delta^2 k_s^2} - 1\right)^{1/2}, \tag{59}$$

where the top sign is for the H branch and the bottom sign for the TG branch. For $\delta \to \infty$, both waves are evanescent with a skin number that is just k_s when $k = k_z = 0$. If $|k| < 2\,\delta k_s$, T^2 is complex, and both waves are ''overstable;'' that is, they propagate with decreasing amplitude. However, if $|k| > 2\,\delta k_s$ and $\delta > \frac{1}{2}$, then $|k| > k_s$ and T^2 is real. Defining $\kappa \equiv k^2/k_{\min}^2 = (k/2\delta k_s)^2$, we can write Eq. (60) as

$$\frac{T^2}{k_s^2} = \kappa - 1 \mp 2\kappa\left(1 - \frac{1}{\kappa}\right)^{1/2}. \tag{60}$$

For $\kappa > 1$, this function is negative for the H wave and positive for the TG wave. We thus redefine T_1 for the H wave as

$$T_1^2 \equiv k^2 - \beta_1^2 > 0, \tag{61}$$

and solve Eq. (26) for this case. The solution that is finite at $r = 0$ is

$$B_1^R = \sqrt{2}A_1(k + \beta_1)I_{m-1}(T_1 r),$$

$$B_1^L = \sqrt{2}A_1(k - \beta_1)I_{m+1}(T_1 r),$$

$$B_{1z} = 2iA_1 T_1 I_m(T_1 r), \tag{62}$$

where I_m is the Bessel function of an imaginary argument. The relative coefficients of B^R, B^L, and B_z were obtained from the components of the parent equation, Eq. (25). For the TG wave, Eqs. (45)–(47) are valid, and the exterior solution is given by Eqs. (48)–(50). Continuity of B^R, B^L, and B_z at $r = a$ then yields the same condition as Eq. (52),

$$A_2 = -A_1\,\frac{f_1 + g_1 - h_1}{f_2 + g_2 - h_2}, \tag{63}$$

but with the new definitions

$$\begin{Bmatrix} f_1 \\ g_1 \end{Bmatrix} = (k \pm \beta_1)\,\frac{I_{m\mp1}(T_1 a)}{K_{m\mp1}(T_3 a)},$$

$$h_1 = -\frac{2k}{T_3}\left(T_1\,\frac{I_m(T_1 a)}{K_m(T_3 a)}\right), \tag{64}$$

while f_2, g_2, and h_2 are still correctly given by Eq. (53). As for the continuity of E_z, the exterior solution is given by Eq. (55), while the new interior expression is

$$E_z^{\text{in}} = \frac{2c^2}{\omega}\,\frac{k_0^2}{k_s^2}\,[A_1\beta_1 T_1 I_m(T_1 a) - A_2\beta_2 T_2 J_m(T_2 a)]. \tag{65}$$

The boundary conditions have the same form as Eqs. (56) and (57), except that now it makes sense to normalize to $A_2 = 1$, and the definitions of Eq. (64) are to be used:

$$C_1 - C_2 = -\frac{k_0^2}{kk_s^2}\,(A_1\beta_1 h_1 + \beta_2 h_2), \tag{66}$$

$$C_1 - C_2 = A_1(f_1 - g_1) + f_2 - g_2. \tag{67}$$

These equations can be satisfied simultaneously only for certain values of k. Figure 13 shows an example of a TG wave coupled to an evanescent H wave for $\omega/\omega_c > \frac{1}{2}$.

IX. SUMMARY AND DISCUSSION

We have investigated the behavior of undamped normal modes of helicon waves in a uniform plasma filling an infinitely long conducting or insulating cylinder. When finite electron mass is taken into account, a second branch of the dispersion relation appears. This is an electron cyclotron wave (Trivelpiece–Gould mode) with short radial wavelength, propagating primarily inward from the radial boundary. Strictly speaking, the boundary conditions in the absence of collisions cannot be satisfied with either wave alone; hence, both waves are excited simultaneously and are linearly coupled at the boundary. At high magnetic fields such that $\delta = \omega/\omega_c \ll 1$, the possible values of the parallel wave number k are quantized by a conducting boundary, with a typical normal mode consisting of a helicon wave of low radial wave number coupled to a TG wave of high radial wave number. However, since the TG wave is expected to be highly damped, its rapid radial variations may not be detectable; and measurements of the wave fields away from the surface are expected to reveal the helicon branch alone. Computations show that the radial profile of the helicon branch is not affected by the presence of the TG branch, in agreement with observations.[18] Thus, earlier theories[3] fortuitously gave very nearly the correct result, but without adequate justification.

In this section, the physical interpretation of our present results, as well as the geometries chosen for study, is based on damping and excitation calculations appearing not in this paper but in the work of Shamrai and Taranov[21,22] and in our own work (part II). For instance, for the case of large B_0, the quantization of the values of k is not physically meaningful, since the damping of the TG component is too strong for its behavior at $r = 0$ to play an important role. On the other hand, the case of small B_0 may be quite different. At low magnetic fields such that $\delta > \frac{1}{2}$, only evanescent helicon modes can exist. For $\delta \leqslant \frac{1}{2}$, the helicon and TG branches have similar radial wave numbers and should be strongly coupled. Though the helicon wave field still has the radial behavior predicted by simple theory,[3] the coupled helicon and TG mode has a different radial profile, which should be measurable in future experiments. Furthermore, the coupling profoundly affects the energy absorption.[22]

When the boundary is an insulating cylinder, the existence of an external field permits the boundary conditions to be satisfied with many values of k, as long as they lie within a range that depends on n_0 and δ. The eigenvalues of k for the conducting boundary case lie within this range. However, for an insulating cylinder the dominant values of k are not determined so much by the boundary conditions as by the efficiencies of excitation and damping at various values of

k. This result is in contradiction with previous expectations[3] that the value of n_0/B_0 is determined by the dispersion relation for given k. It appears that helicon waves can propagate during the buildup of the plasma, even at densities lower than the optimum value.

Though the numerical examples given here are for the $m=+1$ azimuthal mode, the formulas are for arbitrary integer values of m. Study of the constant-density normal modes alone has not given any insight into the reason for the difficulty in exciting the $m=-1$ mode,[18] but it will be shown in part II that antenna coupling is significantly different for the $m=+1$ and -1 modes when the density is peaked on axis.

As has been pointed out by Shamrai and Taranov,[20] consideration of the TG wave completely changes our previous concept of how helicon waves are damped. We have shown here that helicon waves are rigorously undamped in the $m_e=0$ limit. Previous calculations[3] of the damping rate were based on a perturbation scheme that evaluated the lowest-order finite-m_e effects in the parallel motion of the electrons. That method was shown to predict correctly the damping rate of helicon waves in the downstream region away from the antenna.[19] On the other hand, it was found experimentally that the absorption of rf energy occurred almost entirely in the upstream region near the antenna.[23] The new picture that emerges is that absorption of helicon waves occurs via mode coupling to the TG wave at the boundary, followed by strong damping of the TG wave. This mechanism should lead to enhanced deposition of energy near the walls, rather than at the radius where B_z^2 is peaked, leading to a more uniform plasma density profile. Careful experiments in the near-field region are needed to confirm this picture.

ACKNOWLEDGMENTS

This work was supported by the National Science Foundation, Grant No. ECS-9400849; the Semiconductor Research Corporation, Project No. IJ-529; the Livermore Plasma Physics Research Institute, Work Order No. B294691; and the Wisconsin Engineering Research Center for Plasma-Aided Manufacturing.

[1] M. A. Lieberman and R. A. Gottscho, ''Design of high density plasma sources for materials processing,'' in *Physics of Thin Films* (Academic Press, New York, 1994).
[2] F. F. Chen, Phys. Plasmas **3**, 1783 (1996).
[3] F. F. Chen, Plasma Phys. Control. Fusion **33**, 339 (1991).
[4] I. D. Sudit and F. F. Chen, Plasma Sources Sci. Technol. **4**, 43 (1996).
[5] A. R. Ellingboe and R. W. Boswell, Phys. Plasmas **3**, 2797 (1996).
[6] A. Komori, T. Shoji, K. Miyamoto, J. Kawai, and Y. Kawai, Phys. Fluids B **3**, 893 (1991).
[7] S. Shinohara, Y. Miyauchi, and Y. Kawai, Plasma Phys. Control. Fusion **37**, 1015 (1995).
[8] J. P. Klozenberg, B. McNamara, and P. C. Thonemann, J. Fluid Mech. **21**, 545 (1965).
[9] H. A. Bleven, P. J. Christiansen, and B. Davies, Phys. Rev. Lett. **28**, 230 (1968).
[10] R. W. Boswell, Aust. J. Phys. **25**, 403 (1972).
[11] R. W. Boswell, J. Plasma Phys. **31**, 197 (1984).
[12] W. P. Allis, S. J. Buchsbaum, and A. Bers, *Waves in Anisotropic Plasmas* (MIT Press, Cambridge, MA, 1963); F. F. Chen, Phys. Fluids **8**, 1323 (1965).
[13] F. F. Chen, Phys. Fluids **8**, 1323 (1965).
[14] F. F. Chen, M. J. Hsieh, and M. Light, Plasma Sources Sci. Technol. **3**, 49 (1994).
[15] T. H. Stix, *Theory of Plasma Waves* (McGraw-Hill, New York, 1962).
[16] F. F. Chen, *Introduction to Plasma Physics and Controlled Fusion*, 2nd ed., Vol. 1: Plasma Physics (Plenum, New York, 1984), Appendix B.
[17] A. W. Trivelpiece and R. W. Gould, J. Appl. Phys. **30**, 1784 (1959). The dispersion relation given there is $T^2=-k^2(\omega^2-\omega_p^2)(\omega^2-\omega_c^2)/\omega^2(\omega^2-\omega_p^2-\omega_c^2)$. In the limit $\omega_p \gg \omega$, this reduces to $T^2+k^2=k^2\omega_c^2/\omega^2$, which is the same as Eq. (27). The higher-frequency branch (the plasma wave) is not relevant in this case.
[18] M. Light and F. F. Chen, Phys. Plasmas **2**, 1084 (1995).
[19] M. Light, I. D. Sudit, F. F. Chen, and D. Arnush, Phys. Plasmas **2**, 4094 (1995).
[20] K. P. Shamrai and V. B. Sharanov, Plasma Phys. Control. Fusion **36**, 1719 (1994).
[21] K. P. Shamrai and V. B. Sharanov, Phys. Lett. A **204**, 139 (1995).
[22] K. P. Shamrai and V. B. Sharanov, Plasma Sources Sci. Technol. **5**, 474 (1996).
[23] I. D. Sudit and F. F. Chen, Plasma Sources Sci. Technol. **5**, 43 (1996).